ISSN: ISSN: 0974-5823 Vol. 7 No. 2 February, 2022

International Journal of Mechanical Engineering

A theoretical and experimental study with a different load use Lev Palm and two types Nano (Alumina, silicon carbide) addition on abrasive Wear Rate Using Semi-metallic-organic Functionally Graded Materials.

Mothanna Taha Fattah Agha, Shaker S. Hassan, Samir Ali Amin

Department of Mechanical Engineering, University of Technology, Baghdad, Iraq.

Abstract

This study presents the development of a modern semi-metal organic composite; functionally graded depending on nanomaterials 'Alumina or silicon carbide'. During this research, the wear rate, the resistance of wear rate, and specific wear rate were all modified, using a natural lev palm in functionally graded materials and other additives. The nanomaterials are the new technique used in this work to improve the resistance of wear. Lev Palm is the best natural fiber as alternate research used to modify the strength. Hence, lev palm has unique characteristics to be used as filler. In the laboratory, many formulations have been prepared with the percentage weight of lev palm, friction improves, nanomaterials as abrasive materials, softener additive, and other lubricant solid materials. Powder metallurgy technique was used to manufacture the model including lev palm. A theoretical analysis using Buckingham Pi theory was developed in this work, for experimental study, A pin-on-disc under dry test was used to improve the wear rate, specific wear rate, and wear resistance depending on slide distance with a tow of the constant load of '10,30N' and constant speed of 300 rpm. The results showed that the sample (S3) has the best mechanical properties such as wear rate, specific wear rate, and wear resistance.

Keywords: Functionally graded materials (FGMs); Lev palm; Wear test; Nano Alumina; Pin on disk; Buckingham Pi; Composite.

1. Introduction

Many machine components have abrasive interactions between surfaces that cause wear. Grinding, for example, necessitates some abrasive wear. Others, such as bearings, are meticulously maintained to minimize excessive looseness [1], The presence of stick-slip phenomena during the wear process, such as multi-directional abrasion, may exacerbate wear look like in ball joint [2]. Breaking system is the most important part in the automotive, vehicle and machinery; however, brake pad is the major component of the system. Brake pads convert the kinetic energy of the vehicle into thermal energy by friction. For many years, brake pads were constructed of asbestos fiber, which is extremely hazardous in a variety of ways [3]. At the moment, brake pads are categorized as metallic, semi-metallic, and the novel organic composite brake pad materials are commercially available. In industrial pad, many things are found, such as elastomers, ceramic particles, metallic chips, minerals, fibers, and solid lubricants. Most of these things are combined together by phenolic resin [4]. There are tiny quantities that are transferred to the pad or the disc whenever the bad is heated due to the direct contact between the rotating disc and the pad to produce the stopping force. Therefore, there is no single material can accomplish the high performance, which is required to achieve safety and durability

under varied brake situations in a disc brake system [5]. Many researches have been investigated in the area of modifying the asbestos-free brake pads. The use of coconut shell, palm kernel shell (PKS) has been developed for asbestos free brake pads materials[6]–[9]. Natural fibers have greater benefits than inorganic materials, such as low cost, biodegradability, and low density. Natural fibers also have a lower environmental effect than synthetic fibers[10]. Today, many researchers are concentrating on such a way to use industrial/ agricultural trash as an exporter of materials in the manufacturing business. So, the natural organic materials are not only be used for economical purposes, but also result in earnings and environmental things. Non-Asbestos Organic Brake Pads using functionally graded materials technique is presented in this work.

The goal of this paper is comparing the theoretical and experimental result with two different added nano materials to develop novel organic functional graded composite materials for brake pads for automobiles. Functionally graded materials (FGMs) have unique characteristics and can perform several tasks that identical or homogenous materials cannot[11]. Various laboratory combinations with varied lev palm fiber, abrasive material utilizing nano alumina, friction modifiers, and solid lubricant employing powder metallurgy method were developed in this approach. The wear resistance and specific wear rate of the brake pad material were evaluated as tribological characteristics. The new composites were evaluated in the lab with an adequate percentage ratio between reinforcement weight (% W) and matrix and were found to have a better coefficient of friction and wear resistance due to the improved mechanical properties, increased compressive force ability, and low toxin pollution effect. In the present situation, these qualities make the model suitable in automobile brake pads.

2. Theoretical analysis

The Buckingham Pi model is used to create a mathematical model of wear rate. wear volume, materials density, and hardness were chosen as a repeating parameter, other variable, normal load (N), sliding speed (V) and sliding distance (SD) wear unrepeating [1].

The equation can be expressed as fallowing:

$$\prod = f(\rho, w_v, H\ , N, S_d, v)$$

where,

ρ is the density of sample $= Kg/m^3$

w_v is the wear volume rate = m^3

H is the hardness of sample = $kg/m.s^2$

N is the normal load = $kg.m/s^2$

S_d is the sliding distance = m

v is the sliding speed = m/ s

so,

the number of variables is 6 and the number of dimensions is 3

6-3= 3 the number of Pi set

The first set of the dimensionless equation:

$$\rho^a * {w_v}^b * H^C * N = kg^0 * m^0 * s^0$$

$$(\frac{kg}{m^3})^a * (m^3)^b * \left(\frac{kg}{m.s^2}\right)^c * \left(\frac{kg\ .m}{s^2}\right) = kg^0 * m^0 * s^0$$

This mean:

a+c+1=0

-3a+3b-c+1=0

-2c-2=0

solve the three equations to get a=0, b=-2/3, c=-1

$\prod_1 = \quad w_v{}^{-2/3} * \quad H^{-1} * N$

$\prod_1 = \quad \frac{N}{w_v{}^{2/3} * \ H}$ _____ (1)

The second set of the dimensionless equation:

$\rho^a * w_v{}^b * H^C * S_d = kg^0 * m^0 * s^0$

$(\frac{kg}{m^3})^a \ * (m^3)^b * \ \left(\frac{kg}{m.s^2}\right)^c * \ \ (m) = kg^0 * m^0 * s^0$

a+c=0

-3a+3b-c+1=0

-2c=0

or, c=0, a=0, b=-1/3

so, $\prod_2 = \quad w_v{}^{-1/3} * \quad S_d$

$\prod_2 = \quad \frac{w_v{}^{1/3}}{S_d}$ _____ (2)

The 3rd set of the dimensionless equation:

$\rho^a * w_v{}^b * H^C * v = kg^0 * m^0 * s^0$

$(\frac{kg}{m^3})^a \ * (m^3)^b * \ \left(\frac{kg}{m.s^2}\right)^c * \ \left(\frac{m}{s}\right) = kg^0 * m^0 * s^0$

a+c=0

-3a+3b-c+1=0

-2c-1=0

or, c=-1/2, a=1/2, b=0

$\prod_3 = \quad \rho^{1/2} * \quad H^{-1/2} * v$

$\prod_3 = \quad \sqrt{\frac{\rho}{H}} * \quad v$ _____(3)

From equation (1) and (2) to become the following:

$\frac{N}{w_v{}^{2/3} * \ H} \approx \quad \frac{w_v{}^{1/3}}{S_d}$

or

$\frac{N}{H} k = \quad \frac{w_v}{S_d}$

$w_v = k \frac{N * S_d}{H}$ _____(4)

where k is the wear coefficient, the equation (4) is well known as Archard's equation.

The equalizing dimensionless of equations (1), (2) and (3), it produced the following:

$$\prod_1 * \prod_3 \approx \prod_2$$

$$\frac{N}{{w_v}^{2/3} * H} * \sqrt{\frac{\rho}{H}} * v \approx \frac{{w_v}^{1/3}}{S_d}$$

by simplified to get volume wear rate as below:

$$w_v \approx N * S_d * \sqrt{\frac{\rho}{H^3}} * v$$

$$w_v = \beta N * S_d * \sqrt{\frac{\rho}{H^3}} * v \quad \text{_____(5)}$$

where β is the wear speed coefficient.

finally, to compute the wear rate with loose mass, equation (5) can be modified by following

$$w_m = \beta N * S_d * \sqrt{\frac{\rho^3}{H^3}} * v$$

$$w_m = \beta N * S_d * \left(\frac{\rho}{H}\right)^{3/2} * v \; v \quad \text{_____(6)}$$

where w_m is the mass wear rate.

β is the wear speed coefficient and taken according [1].

Equation (6) will be used to compare the result of experimental wear rate.

3. **Experimental Procedure**

3.1. **Materials and Methods**

Lev are collected from Iraqi palms that are naturally accessible (see Figure 1), chopped, and dried at room temperature to eliminate the humidity. The obtained lev was immersed in a 5 percent alkali solution NaOH for one hour before being washed with water to remove any remaining solution and then dried again by using laboratory oven at 50° C used for the preparation of composite samples. The Lev palm acts as a filler and reinforcement. Other materials and equipment used during this work are: phenolic resin (Novolac and Hexamine hardener) as a binder material (Matrix), Iron (Fe) as friction modifiers, Nano Alumina as abrasive, graphite (800 Mesh) as a solid lubricant, and Aerosol as a soften material. All materials were in powder state, and their high coefficient of friction and low wear rate, while maintaining mechanical strength, are important aspects to consider while choosing these materials. In order to generate functionally graded materials, careful analysis of the required attributes of distinct layers of mixed materials was performed.

Figure 1. Extracted lev palm

3.2. **The Mould Preparation**

The mould was manufactured using a stainless-steel plate with a dimension of specimen (150*50) mm. The mould consists of three parts of hard plate (top and bottom) and frame to be held together. The mould looks like a piston and prevents the mixture to release out when being pressed, as shown in Figure 2.

Figure 2. The Mould Parts

3.3. **Specimen Preparation**

A fat layer acts as a demoulding agent and is applied to the mould initially. An aluminum foil is also employed to guarantee that the surfaces of the samples are smooth.

After dring the lev palm, cutting and crusher using high speed multi-functional crusher with rotating speed (25000) rpm (see Figure 3) and the final product (see Figure 4) as a powder slag. The composition of the lev palm composites used in this work is shown in Table 1.

Figure 3. High Speed Multi-Functional Crusher

Figure 4. Lev palm powder slag

The specimens consist of two layers, every layer contains a percentage (%W) of materials to get a gradually characteristic in the model.

A technique called powder metallurgy was employed in making the test specimen[12]. The ingredients' compounded weight percentages were modified using the trial and error approach. Every sample consists of two layers of compounded materials, and

every layer was mixed individually using hand layup mixture material.After preparing the mould, the first layer was put with a uniform distribution and a hand pushing pressure by using the top part of mould, and then the second layer will act.

Table 1. Material percentage (%wt) in the composite brake pad material.

Layers	Materials	Formulations of specimens in weight percentages (% wt)			
		S1	**S2**	**S3**	**S4**
1	Lev palm powder	25	25	20	20
	Phenolic resin powder	40	40	40	40
	Graphite	10	8	10	10
	Nano Alumina Al2O3	0	8	12	0
	Silicon Carbide SiC	0	0	0	12
	Aerosol	15	10	10	10
	Iron	10	9	8	8
2	Lev palm powder	30	30	30	30
	Phenolic resin powder	40	40	40	40
	Graphite	8	8	8	8
	Nano Alumina Al2O3	0	0	0	0
	Silicon Carbide SiC	0	0	0	0
	Aerosil	10	10	10	10
	Iron	12	12	12	12

Using a hydraulic cold press, compression moulding machine, a pressing was done with a pressure of 15 MPa at the room temperature (see Figure 5) and 20 minutes later, the pressure reduced to (1-1.5) MPa and the hot press hold at 140°C for about 30 minutes. After that, the plate was cured for 6 hours in the surrounding atmosphere. The plate was created with a dimension of 150 mm x 50 mm and a thickness of 10 mm. Then, according to ASTM standard protocols, the coefficient of friction ,wear resistance and spesific wear rate of these four plates may be determined by tribological testing

Figure 5. Hydraulic Cold-Hot press

As illustrated in Figure 6, a dry test pin-on-disc machine was used to analyze the wear rate, specifically the wear rate of the sliding contact surfaces of specimens. The tests were carried out in a dry laboratory setting according to the ASTM G99-95 standard[13].

The specimen was prepared from cutting the plate sample and fixed with a rotating disk specimen with 20 mm dimeter.

Figure 6. Pin-on-Disc Wear Machine

The disk specimen was previously cleaned with acetone before being correctly weighed on a electronic digital scale with accuracy of 0.0001 g. The experimental test was done on two type of normal loads of 10 N and 30 N.were applied and the test was repeated for varied time 5, 10, 15, 20,25, and 30 minute and then converted to sliding distances. The disc specimen can be rotated with a contact radius of 5.5 mm, at a constant speed of 300 rpm. Tool steel with a hardness of 385 HV was used for the pin ball. The weight of specimen before and after one route was measured.

Hardness of the functionally graded composite samples was measured, according to DIN 53505 and ISO 868 using a Shore D equipment (Karl Frank GmbH, Type 104, Germany)[14]. Hardness measurements were obtained from multi different points on each sample, and then the arithmetic average was taken into account[15].

The wear rate (W) was estimated using the following equation from the volume loss resulting from the mass loss of specimen [16]:

$$Wear\ \ rate\ \left(\frac{mm^3}{m}\right) = \frac{Mass\ \ loss(g)}{\rho(g/mm^3) * D_S(m)} \quad (7)$$

Where, ρ is the density of material (g/mm^3) and D_S is the sliding distance (m).

The specific wear rate (W_s) was also obtained by diving the wear rate on the applied load (10, 30 N) respectively.

3. Results and Discussion

3.1. Wear Rate And Specific Wear Rate According Sliding Distance

Figure 7 depict the sliding distance effect on wear rate, with applied constant load (10 N) and constant speed (300 rev/min). Samples S3 and S4 show the nearest behavior regarding the same percentage %w added of nano materials.

Figure 8 depict the sliding distance effect on specific wear rate, with applied constant load (10 N) and constant speed (300 rev/min). Samples S3 and S4 show the nearest behavior regarding the same percentage %w added of nano materials.

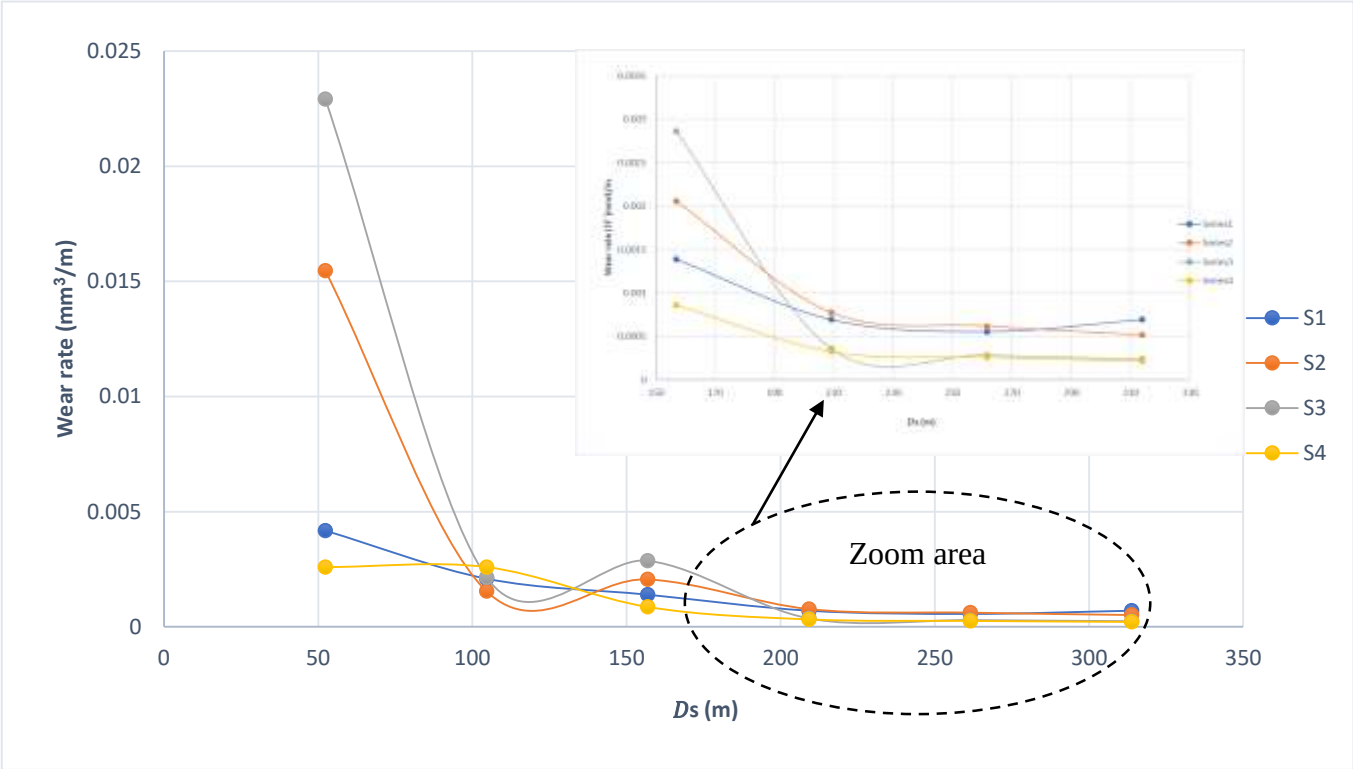

Figure 7. Wear rate (mm^3/m) with applied constant load (10N) and constant speed (300 rev/min).

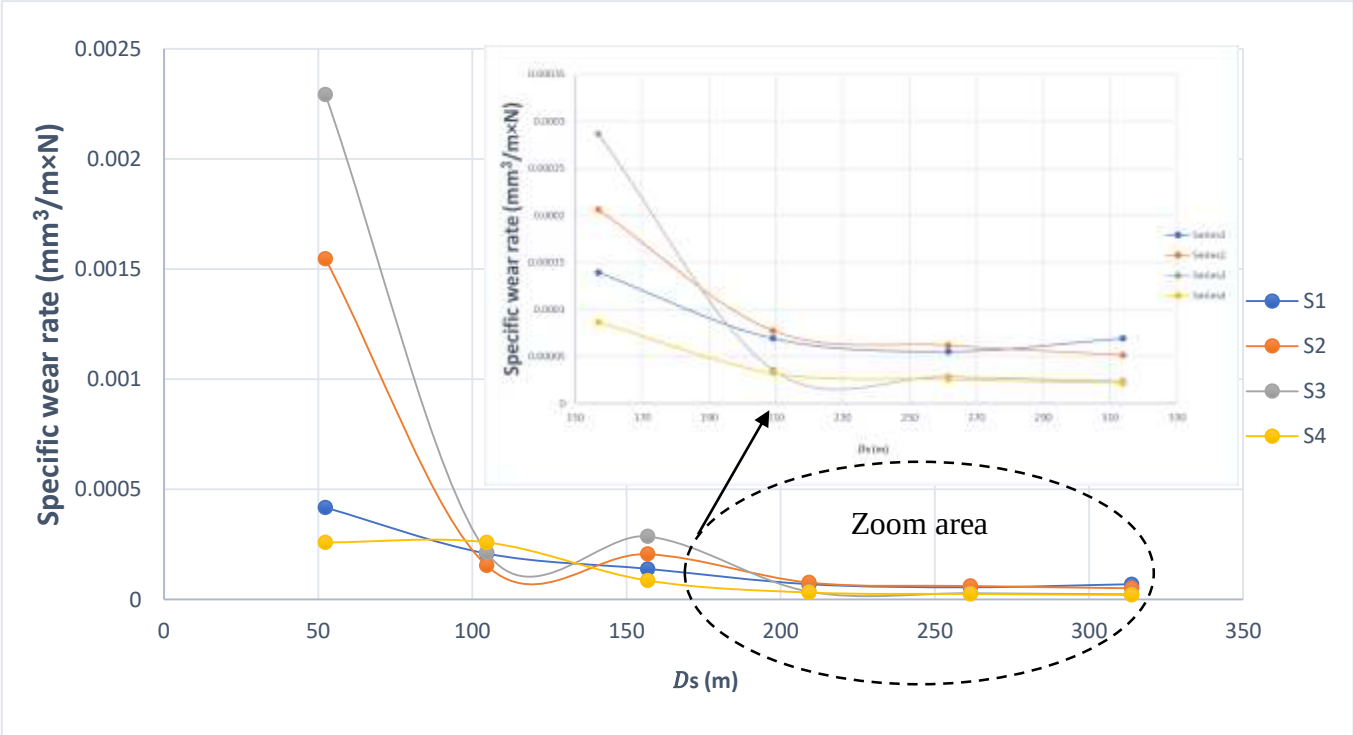

Figure 8. Specific wear rate (mm3/m×N) with applied constant load (10N) and constant speed (300 rev/min).

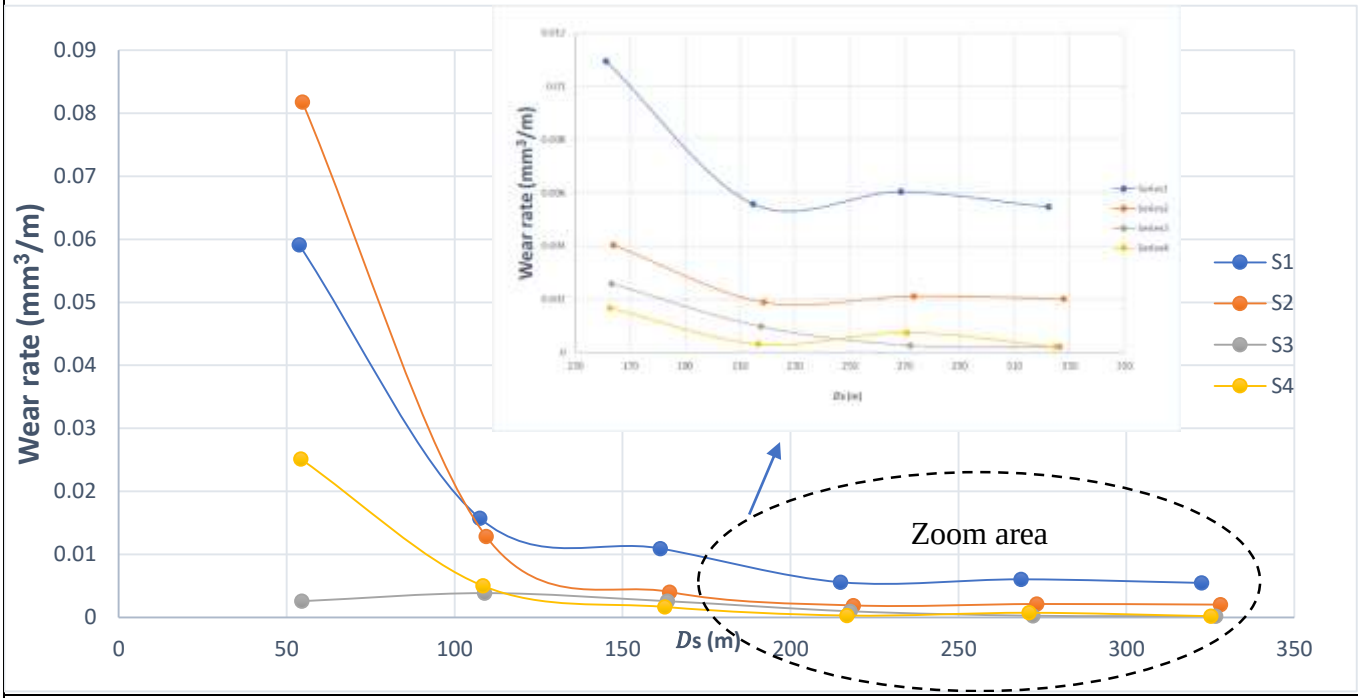

Figure 9. Wear rate (mm^3/m) with applied constant load (30N) and constant speed (300 rev/min).

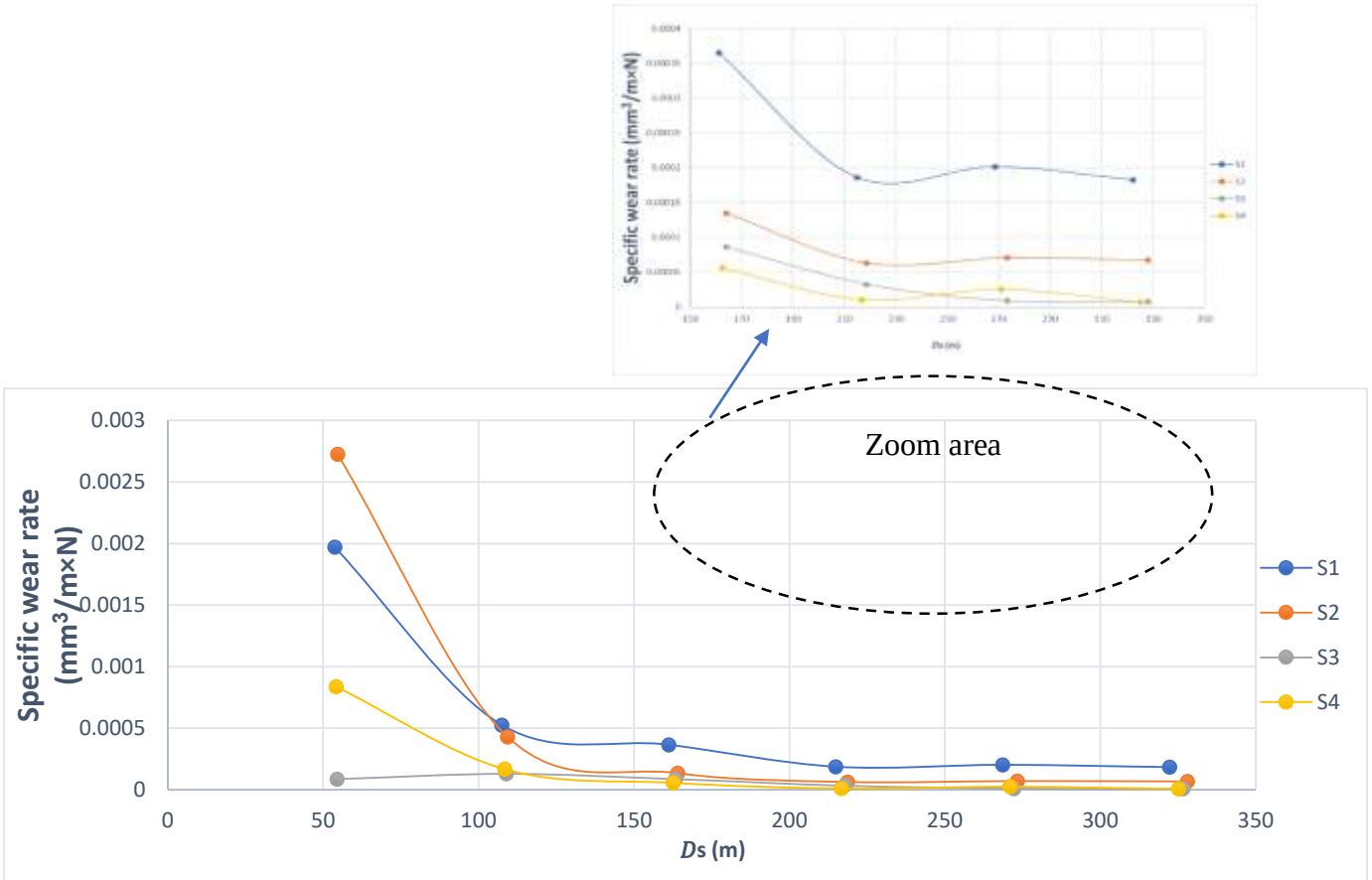

Figure 10 Specific wear rate ($mm^3/m \times N$) with applied constant load (30N) and constant speed (300 rev/min).

Figures 9 and 10 depict the sliding distance effect on wear rate and specific wear rate respectively, with applied constant load (30 N) and constant speed (300 rev/min).

very closely behavior that found with load of 30 N and the pattern similar to previously loaded. stay sample S3 and S4 have nearest value.

Figures 11,12,13,14,15,16,17,18,19,20,21,22,23,24,25 and 26 depict the sliding distance effect on wear rate and specific wear rate comparison between experimental and theoretical result in each sample and with different load applied once 10 N and other 30 N.

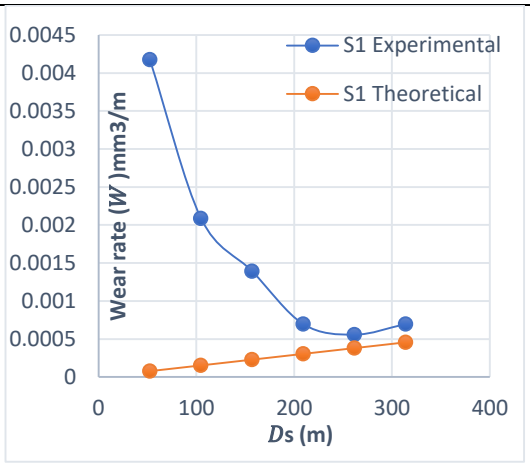

Figure 11. Wear rate of S1 Experimental and Theoretical applied to 10 N load.

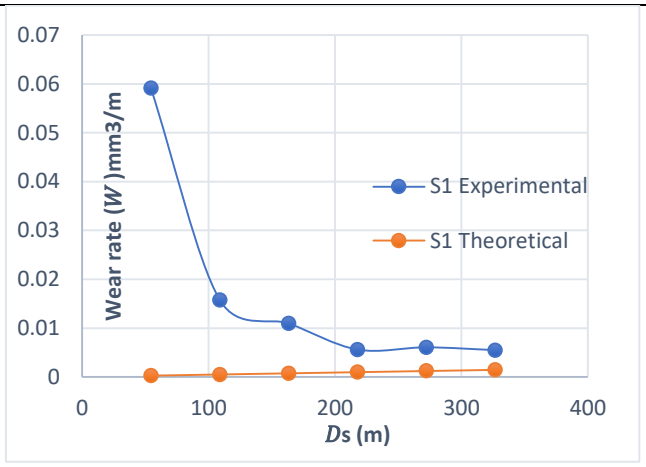

Figure 12 Wear rate of S1 Experimental and Theoretical applied to 30 N load.

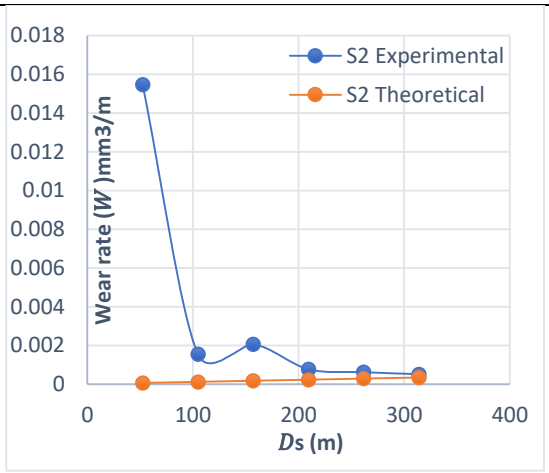

Figure 13. Wear rate of S2 Experimental and Theoretical applied to 10 N load

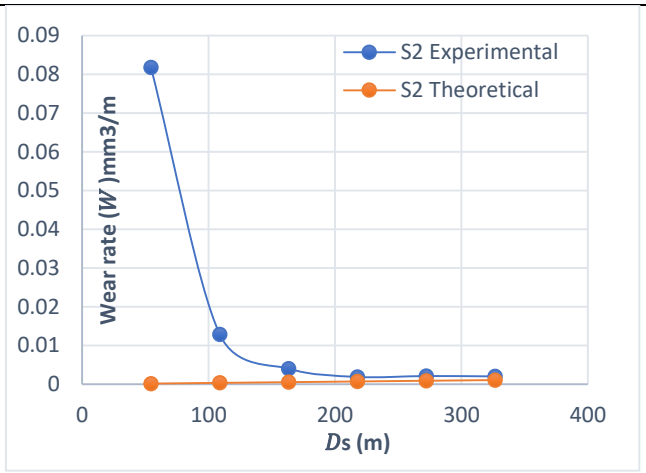

Figure 14. Wear rate of S2 Experimental and Theoretical applied to 30 N load.

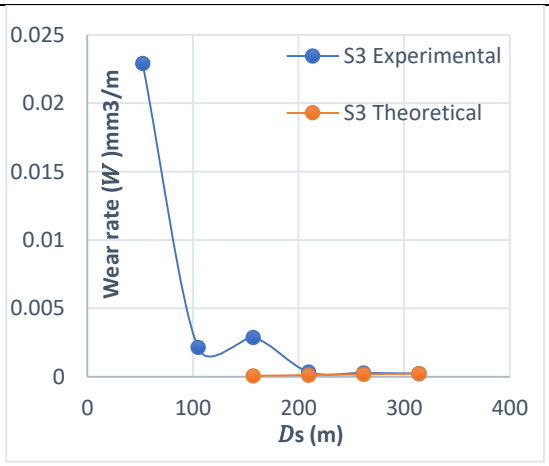

Figure 15. Wear rate of S3 Experimental and Theoretical applied to 10 N load

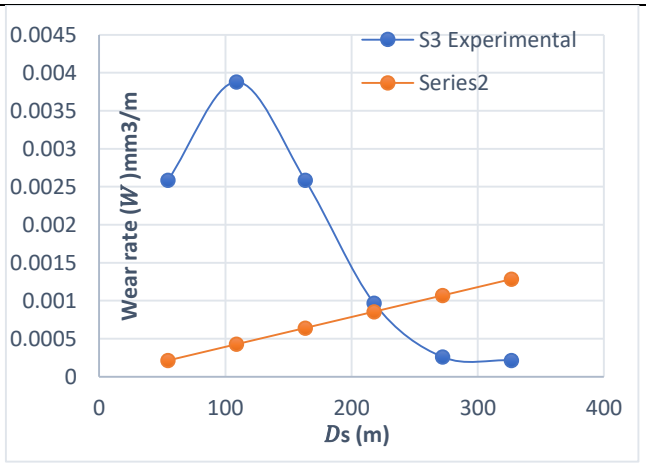

Figure 16. Wear rate of S3 Experimental and Theoretical applied to 30 N load.

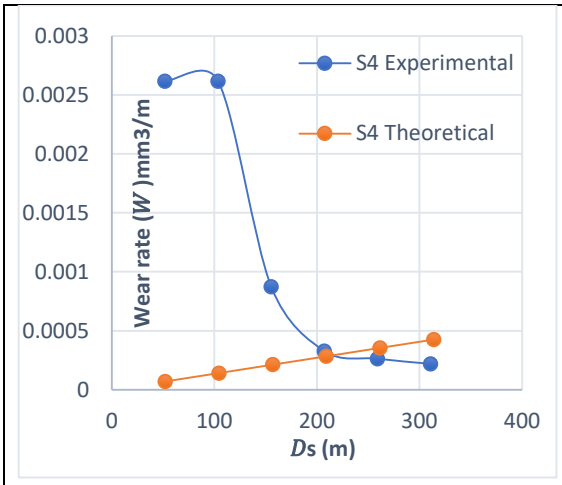

Figure 17. Wear rate of S4 Experimental and Theoretical applied to 10 N load

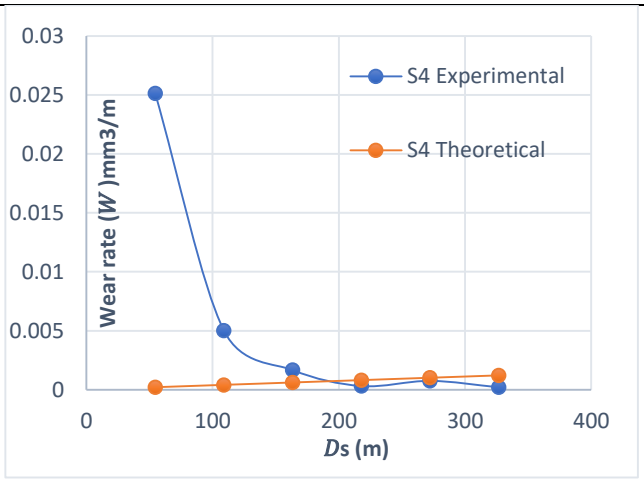

Figure 18. Wear rate of S4 Experimental and Theoretical applied to 30 N load.

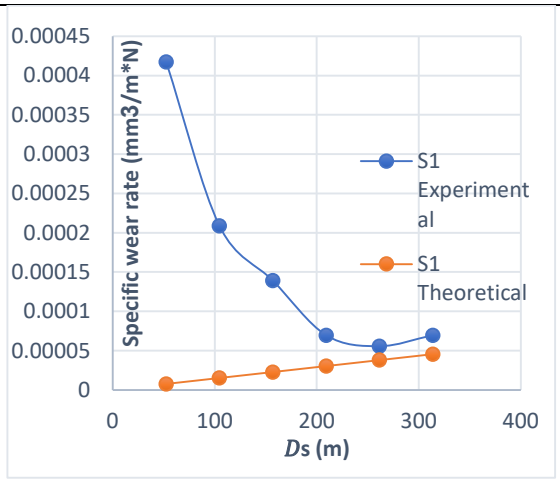

Figure 19. Specific wear rate S1 Experimental and Theoretical applied to 10 N load

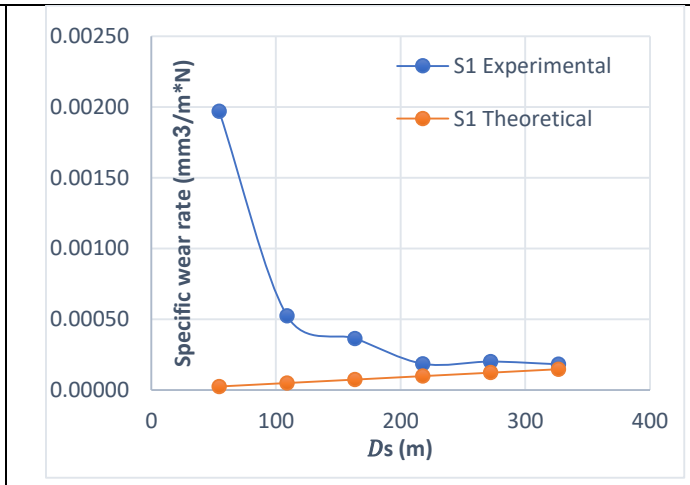

Figure 20. Specific wear rate S1 Experimental and Theoretical applied to 30 N load

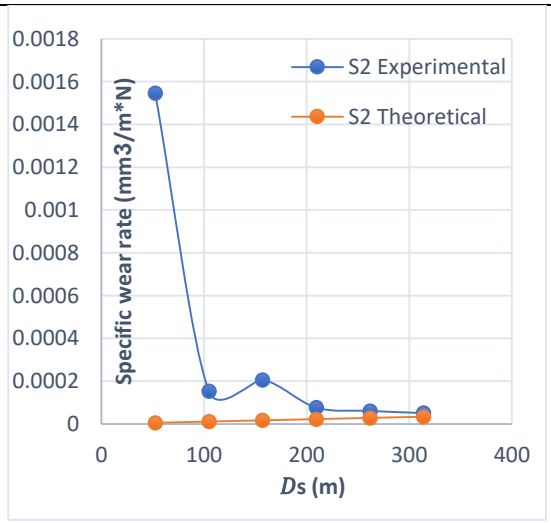

Figure 21. Specific wear rate S2 Experimental and Theoretical applied to 10 N load

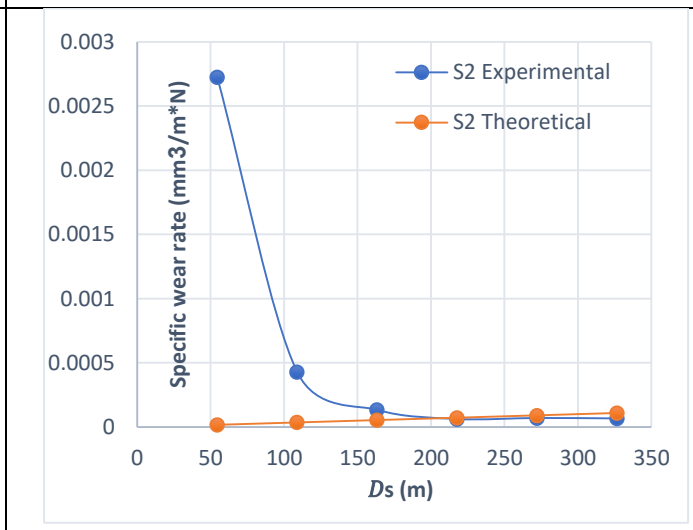

Figure 22. Specific wear rate S2 Experimental and Theoretical applied to 30 N load

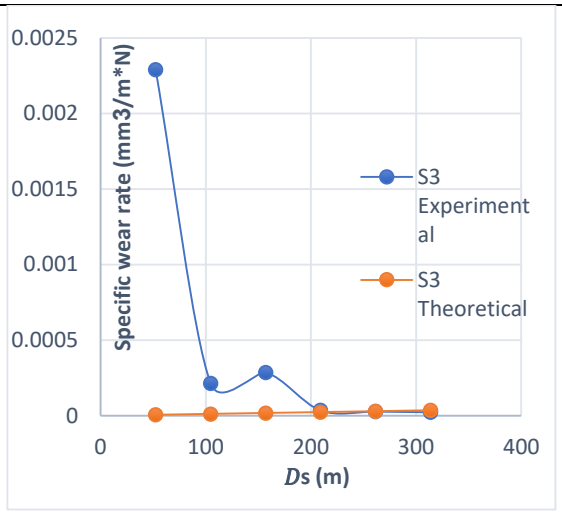

Figure 23. Specific wear rate of S3 Experimental and Theoretical applied to 10 N load

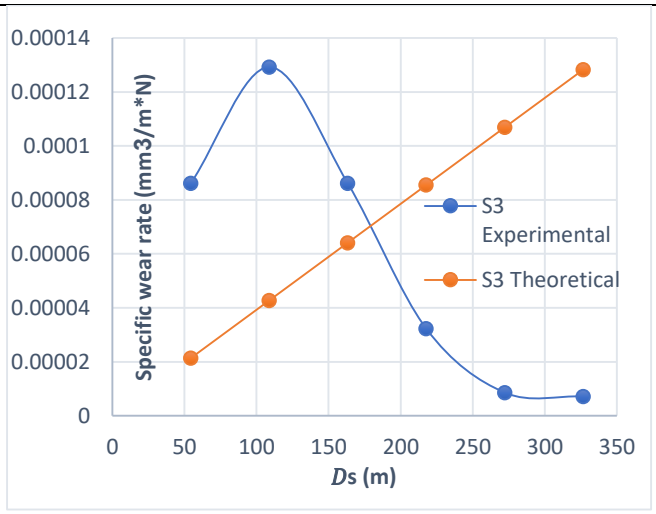

Figure 24. Specific wear rate S3 Experimental and Theoretical applied to 30 N load

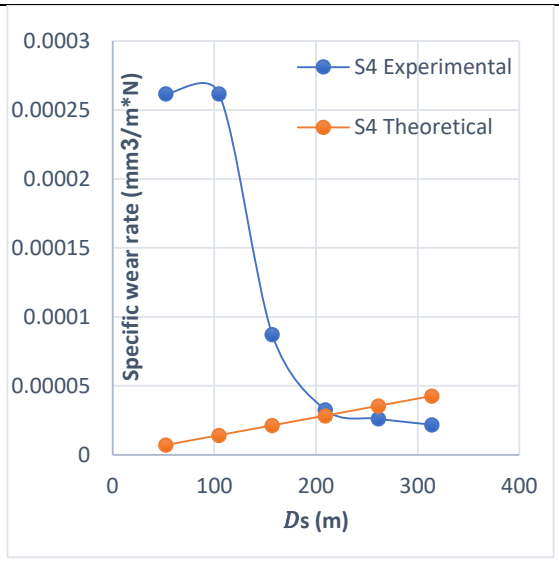

Figure 25. Specific wear rate of S4 Experimental and Theoretical applied to 10 N load

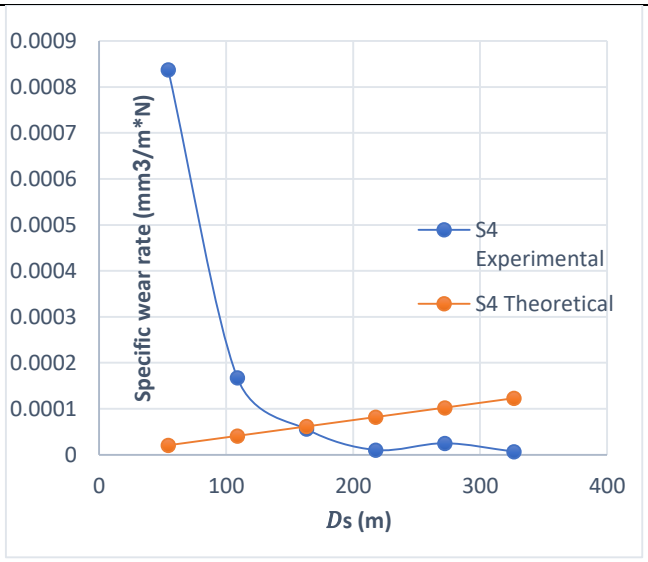

Figure 26ss. Specific wear rate of S4 Experimental and Theoretical applied to 30 N load

Table 2 and 3 show the parameter for wear rate and specific wear rate respectively in experimental and theoretical results, with a constant load of 10 N and constant speed of 300 rpm.

Table 2. The wear rate values of the used parameters of pin-on-disc wear test and theoretical results.

Time (s)	SD =s*t (m)	Wear rate (mm^3/m)							
		S1		S2		S3		S4	
		Theo	Exp	Theo	Exp	Theo	Exp	Theo	Exp
300	52.31	0.00008	0.00417	0.00006	0.01546	0.00006	0.02291	0.00008	0.0026
600	104.6	0.00015	0.00209	0.00011	0.00154	0.00012	0.00215	0.00015	0.0026
900	156.9	0.00023	0.00139	0.00017	0.00206	0.00018	0.00286	0.00023	0.00087
1200	209.23	0.00030	0.00069	0.00023	0.00077	0.00024	0.00036	0.00030	0.00033
1500	261.54	0.00038	0.00056	0.00029	0.00062	0.00030	0.00029	0.00038	0.00026
1800	313.84	0.00046	0.00069	0.00034	0.00052	0.00036	0.00024	0.00046	0.00022

Table 2. The specific wear rate values of the used parameters of pin-on-disc wear test and theoretical results.

Time (s)	SD =s*t (m)	Specific wear rate $mm^3/m*N$							
		S1		S2		S3		S4	
		Theo	Exp	Theo	Exp	Theo	Exp	Theo	Exp
300	52.31	0.000008	0.00042	0.000006	0.00155	0.000006	0.00229	0.000008	0.00026
600	104.6	0.000015	0.00021	0.000011	0.000151	0.000012	0.00021	0.000015	0.00026
900	156.9	0.000023	0.00014	0.000017	0.000206	0.000018	0.00029	0.000023	0.000087
1200	209.23	0.000030	0.000069	0.000023	0.000077	0.000024	0.000036	0.000030	0.000033
1500	261.54	0.000038	0.000056	0.000029	0.000062	0.000030	0.000029	0.000038	0.000026
1800	313.84	0.000046	0.000069	0.000034	0.000052	0.000036	0.000024	0.000046	0.000022

In Figures.7,8 the wear rate and specific wear rate shows a ‘decreasing -steady state' pattern. For the four distinct pad brake material samples, i.e., S1, S2, S3 and S4. The development of cold welding and rupture of asperities on the raw brake pad surface might have caused the rising trend wear at the commencement of the adhesive dry test. As a result, Because the detached asperities were imprisoned between the sliding surfaces, there was a high relative motion resistance, i.e. a high friction coefficient. As a result, the temperature of the interfaces increased during the test, [5][17] also found similar findings. It was discovered that the test specimen's uneven surface can lead to the formation of a third body between the interfaces. Those third entities can help with film transfer onto the sliding counter face by moving between the interfaces in a circular or linear motion. During the adhesive dry test, this raised the friction coefficient, resulting in a considerably higher contact temperature. When the contact temperature was raised, the friction coefficient of all friction materials began to decrease as a result of frictional heating, or fade. On the contrary, for the three distinct brake pad material samples, there was evidence of a ‘running in' phase of wear rate. The wear rate decrease, and reached to a semi steady state wear rate after 314 sliding distance in meter unit or after 1800 seconds, the pattern of variations in wear performance for the three brake pad material samples shows the similar behaviours. Similar reasons were provided in [18], emphasizing the consistency of the above-mentioned explanations. the properties of lev palm and the abrasive nano alumina that is used in this work make a simultaneous phenomenon to reach to a steady state wear rate. Three body asperities, the rise in temperature and the properties of lev palm smoothing make a filling in the surface of contact, so in the result the friction surface increased and the wear rate decreased.

3.2. Wear Resistanse According to Sliding Distance

Table 4 show the parameter for wear resistance with experimental and theoretical results, with a constant load of 10 N and constant speed of 300 rpmand the Figure 27 display the experimental phenomena of wear resistance with sliding distance.

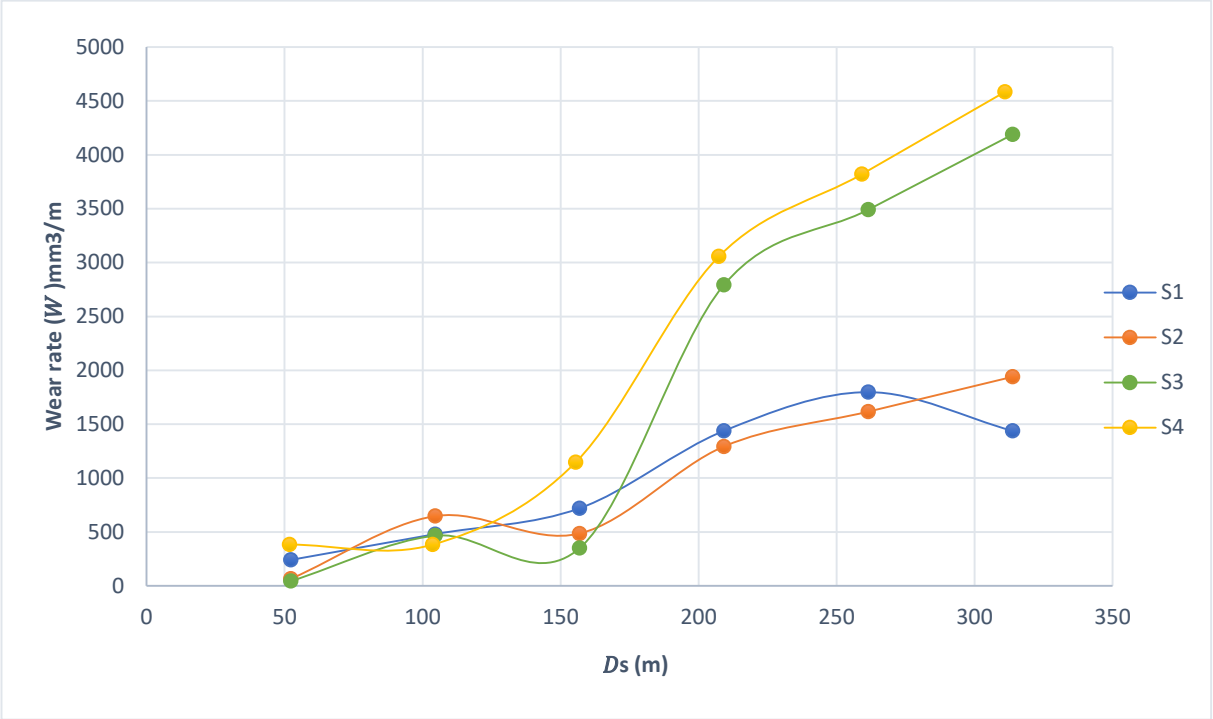

Figure 27. wear resistance (m*N /mm^3) with applied constant load (10 N) and constant speed (300 rev/min).

Table 3. The wear resistance values of the used parameters of ball-on-disc wear test.

Time (s)	**SD =s*t (m)**	**wear resistance (m*N /mm^3)**			
0	0	**S1**	**S2**	**S3**	**S4**
300	52.31	239.6	64.7	43.6	382
600	104.6	479.1	646.6	465.6	382.
900	156.9	718.7	485	349.2	1146.5
1200	209.23	1437.3	1293.2	2793.4	3057
1500	261.54	1796.6	1616.5	3491.7	3821
1800	313.84	1437.3	1939.8	4190.1	4586

The wear resistance in S3 and S2 was increased than S1 by 191% and 35% respectively, the added of nano alumina was cleared effect on wear resistance finally. Figure 14 show the percentage increase of wear resistance.

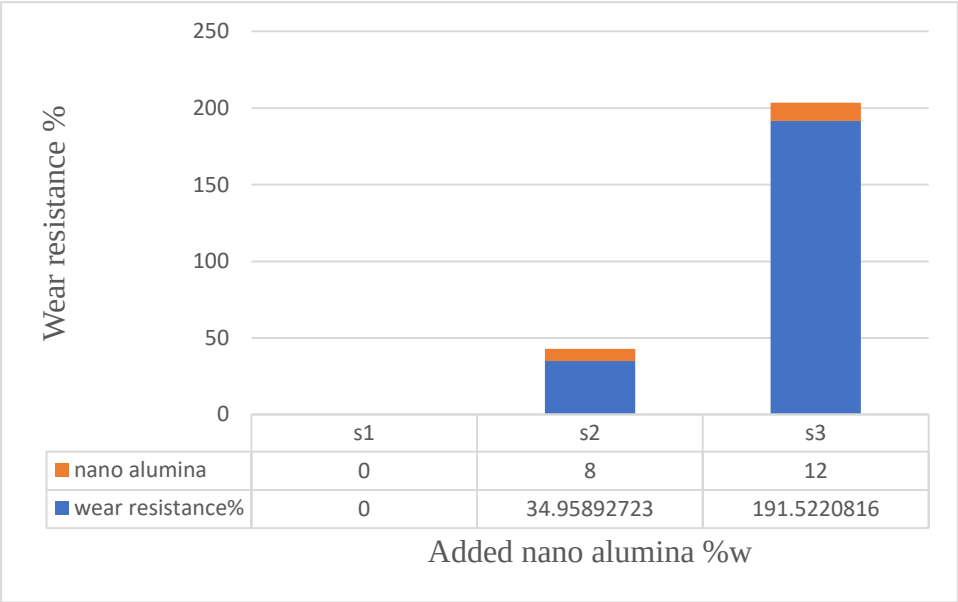

Figure 14. Wear Resistance increase % (m*N /mm^3)

4. Conclusions

Under dry sliding, the effects of sliding distance and the load of pressure contact on the wear rate for three samples were investigated. Pin on disc experiments have been used to investigate the various elements of brake pad material dry sliding wear, cold and hot hydraulic press machine illustrated to make a sample to be test as a FGMs composite pad break, a lev palm is a new filler and reinforcement materials that to be used in this work. The following are the study's and evaluation's conclusions:

(1) When sliding distance was taken into account, the wear rate for all samples showed a ‘’decreasing -steady state’’ pattern. In comparison to the others, S3 had the highest wear rate resistance.

(2) When sliding distance was taken into account, the specific wear rate for all samples showed a ‘’decreasing -steady state’’ pattern. In comparison to the others, S3 had the highest specific wear rate resistance.

(3) The lev palm is very useful to be used as a filler and a reinforcement material to pad break, because of the unique property and the permission to contain the asperities to increase the wear rate resistance and the specific wear rate with sliding distance to reach the steady state trend.

(4) Wear rate of S1 was found less than S2 and S3, by (34%, 191%), (S1< S2 < S3) due to the effect of adding more lev palm and nano alumina %W to sample, and by taking into consideration that S3 have the highest percentage % weight of nano alumina than S1 and S2.

(5) Specific wear rate of S1 was found less than S2 and S3, by (34%, 191%), (S1< S2 < S3) due to the effect of adding more lev palm and nano alumina %W sto sample, and by taking into consideration that S2 have the highest percentage % weight of nano alumina than S1 and S2.

(6) Wear resistance increased in S3 about 116% than S2 and about 191% than S1, and the wear resistance in S2 is increased by 35% than S3, and this increasing issue is regarding the added of nano alumina and ideal mixed percentage weight between the lev palm and nano alumina.

(7) Finally, the equation derived from the Buckingham Pi model mostly applies to non-metallic materials. Sliding speed has a significant impact on wear volume. The greater the speed, the greater the wear mass rate. The hardness and density of the material impact the wear-speed coefficient as a result of the equality process in the Buckingham Pi model.

(8) The best sample that has been investigated is the S3, have the best wear rare, specific wear rate, Hardness and the best wear resistance.

References

[1] Y. Kaelani and A. Syaifudin, "Mathematical model of wear volumes due to sliding speed using Buckingham Pi Model," *IOP Conf. Ser. Mater. Sci. Eng.*, vol. 1034, no. 1, p. 012165, 2021, doi: 10.1088/1757-899x/1034/1/012165.

[2] Y. Kaelani and R. Y. Kurnia, "Identification method for stick slip contact within multi directional contact friction," in *AIP Conference Proceedings*, 2018, vol. 1983, no. 1, p. 50012.

[3] S. Sri Karthikeyan, E. Balakrishnan, S. Meganathan, M. Balachander, and A. Ponshanmugakumar, "Elemental analysis of brake pad using natural fibres," in *Materials Today: Proceedings*, 2019, vol. 16, pp. 1067–1074, doi: 10.1016/j.matpr.2019.05.197.

[4] P. Chandra Verma, L. Menapace, A. Bonfanti, R. Ciudin, S. Gialanella, and G. Straffelini, "Braking pad-disc system: Wear mechanisms and formation of wear fragments," *Wear*, vol. 322–323, no. December, pp. 251–258, 2015, doi: 10.1016/j.wear.2014.11.019.

[5] K. W. Liew and U. Nirmal, "Frictional performance evaluation of newly designed brake pad materials," *Mater. Des.*, vol. 48, pp. 25–33, 2013, doi: 10.1016/j.matdes.2012.07.055.

[6] R. S. Fono-Tamo and O. A. Koya, "Influence of Palm Kernel Shell Particle Size on Fade and Recovery Behaviour of Non-asbestos Organic Friction Material," *Procedia Manuf.*, vol. 7, no. February 2010, pp. 440–451, 2017, doi: 10.1016/j.promfg.2016.12.031.

[7] I. M. Dagwa and A. O. A. Ibhadode, "Design and manufacture of experimental brake pad test rig," *Niger. J. Eng. Res. Dev.*, vol. 4, no. 3, pp. 15–24, 2005.

[8] V. S. Aigbodion, U. Akadike, S. B. Hassan, F. Asuke, and J. O. Agunsoye, "Development of asbestos-free brake pad using bagasse," *Tribol. Ind.*, vol. 32, no. 1, pp. 12–17, 2010.

[9] U. P. Anaidhuno, S. Ologe, F. Maduike, and C. E. Mgbemena, "The Development of Vehicle Brake Pad Using Local Materials - (Palm Kernel, Coconut And Cashew Shells As Base Materials).," *IOSR J. Eng.*, vol. 07, no. 06, pp. 61–67, 2017, doi: 10.9790/3021-0706016167.

[10] A. Lakshumu Naidu and S. Kona, "Experimental study of the mechanical properties of banana fiber and groundnut shell ash reinforced epoxy hybrid composite," *Int. J. Eng.*, vol. 31, no. 4, pp. 659–665, 2018.

[11] M. S. El-Wazery, A. R. El-Desouky, O. A. Hamed, A. Fathy, and N. A. Mansour, "Electrical and mechanical performance of Zirconia-Nickel functionally graded materials," *Int. J. Eng. Trans. A Basics*, vol. 26, no. 4, pp. 375–382, 2013, doi: 10.5829/idosi.ije.2013.26.04a.06.

[12] A. Ibukun Olabisi., "Development and Assessment of Composite Brake Pad Using Pulverized Cocoa Beans Shells Filler," *Int. J. Mater. Sci. Appl.*, vol. 5, no. 2, p. 66, 2016, doi: 10.11648/j.ijmsa.20160502.16.

[13] S. Koksal, F. Ficici, R. Kayikci, and O. Savas, "Experimental optimization of dry sliding wear behavior of in situ AlB2/Al composite based on Taguchi's method," *Mater. Des.*, vol. 42, pp. 124–130, 2012.

[14] A. Szymczyk, E. Senderek, J. Nastalczyk, and Z. Roslaniec, "New multiblock poly (ether-ester) s based on poly (trimethylene terephthalate) as rigid segments," *Eur. Polym. J.*, vol. 44, no. 2, pp. 436–443, 2008.

[15] F. Ficici, S. Koksal, R. Kayikci, and O. Savas, "Investigation of unlubricated sliding wear behaviours of in-situ AlB2/Al metal matrix composite," *Adv. Compos. Lett.*, vol. 20, no. 4, p. 096369351102000404, 2011.

[16] R. A. Kumar, R. K. Kumar, and N. Radhika, "Mechanical and wear properties of functionally graded Cu-11Ni-4Si/graphite composite," *Silicon*, vol. 11, no. 6, pp. 2613–2624, 2019.

[17] U. Nirmal, J. Hashim, S. T. W. Lau, Y. My, and B. F. Yousif, "Betelnut fibres as an alternative to glass fibres to reinforce thermoset composites: a comparative study," *Text. Res. J.*, vol. 82, no. 11, pp. 1107–1120, 2012.

[18] N. S. M. El-Tayeb and K. W. Liew, "On the dry and wet sliding performance of potentially new frictional brake pad materials for automotive industry," *Wear*, vol. 266, no. 1–2, pp. 275–287, 2009.